Oblique impact for flexible robotic finger system

Jiongcan Yang, Yunian Shen

Department of Mechanics and Engineering Science, School of science, Nanjing University of Science and Technology,
yunianshen@njust.edu.cn

ABSTRACT — *A new contact model which takes account of the normal and the tangential compliance of the local contact zone is proposed to depict the oblique impact effect for the flexible robotic finger system in this paper. The criteria for different motion processes for the local compliant contact model (LCCM) is also established. By the use of the proposed LCCM incorporating with absolute nodal coordinate formulation (ANCF), the oblique impact mechanism is analyzed. The results show that multiple transitions between compression and restitution in normal direction appear through an oblique impact event. There exist two motion modes: 1) three times of slip compression-slip restitution when μ≤0.8; 2) stick compression-stick restitution-slip restitution-slip compression-slip restitution when μ≥1.2. In addition, it also shows that falling height, coefficient of friction and energetic coefficient of restitution all have a significant effect on the peak value of contact force and the duration time of contact.*

1   Introduction

One of the greatest challenges in controlling robotic hands is grasping and manipulating objects in unstructured and uncertain environment[1]. The traditional robotic hands are typically too rigid to prevent unexpected impact and subsequent damage. Due to the passive compliance and damping, the flexible robotic hands have great versatility and robustness. The flexible robotic hands are very suitable for the unstructured and uncertain environment. Like the rigid robotic hands, the oblique impact with friction will happen inevitably when a flexible robotic hand grasps things. It will bring vibration with high frequency, the propagation of the transient waves and high amplitude contact force. In the case of repeated impacts, the nonlinear characteristics of periodic motions, quasi-periodic motions, and chaotic motions sometimes will occur in the system. Those characteristics all will lead to many adverse effects such as structural failure, noise increasing and safety decreasing[2]. These phenomenon are similar to oblique impact of vibration of skew bridges[3], metal explosion[4], and etc.

When an oblique impact occurs, the impact structure does not only have a unilateral constraint in the normal direction of the contact surface, but also a frictional constraint in the tangential direction. Djerassi[5] proposes the Stronge's collision hypothesis together with Routh's semi-graphical method to derive an analytical solution to the problem of the oblique impact. Pfeiffer[6] experimentally investigates the energy of a rubber disc oblique impact against a roughness ground. It shows that the energy loss is resulted from that there is a residual deformation at the local contact zone after the impact. The tangential deformation of the contact zone has a significant effect the impact responses of the system. Shen and Stronge[7] propose a lumped parameter contact model which can analyze the reverse sliding of the contact point, and then discuss the effect of contact compliance on the tangential velocity and contact force at the contact point. However, they only take the compliance of the local contact zone into account, the rest of the link is still treated as rigid body. Zaidi[8] proposes a nonlinear mass-spring contact model which is similar to Shen and Stronge's. By the use of the contact model, the tangential and normal contact deformation during slip and stick state is calculated, which is

caused by the rigid finger grasping the flexible object. The transient characteristics in the initial phase of the grasping are neglected. The minimum contact forces are obtained when the hand in a stable grasping state. However, the transient characteristics cannot be ignored once the robotic hand is flexible enough.

In this paper, considering the normal contact compliance and tangential contact compliance, a hybrid analytical model is proposed to study the oblique impact of the flexible robotic finger system. The research focuses on analyzing the tangential and normal relative motion state between fingertip and ground and obtaining the high amplitude contact forces during the oblique impact. In Section 2, the ANCF is used to discrete the deformation field and inertia filed of the finger structure. The hybrid analytical model is introduced and the control equations of the system are derived. In Section 3, the criteria for different motion processes are established, then the numerical integration method is given. In Section 4, various groups of flexible robotic finger system under different parameters are simulated.

2 Hybrid analytical model and control equations

In order to further study the oblique impact effect of the flexible robotic finger system, a hybrid analytical model is developed (see Fig. 1). The hybrid analytical model is composed of a flexible robotic finger system model, a LCCM[9] and a Coulomb friction model. And the flexible robotic finger system is consisted of three flexible links with a half-spherical contact end. Point O is a fixed hinge, and each two phalanges are connected by a revolute joint (see Fig. 1(a)). The finger system is initially in horizontal state, and it will be free falling driven by gravity. Once the drop height of contact end is equal to H, oblique impact occurs with a rigid ground which having a certain roughness. In the following, the control equations based on ANCF for the flexible robotic finger system are derived.
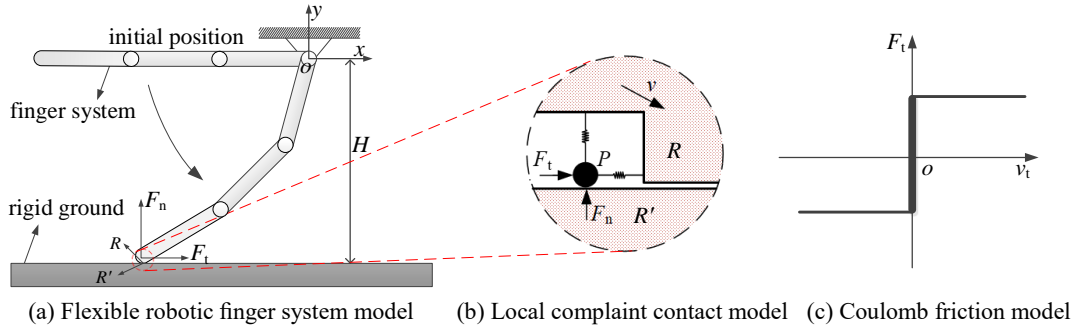

(a) Flexible robotic finger system model   (b) Local complaint contact model   (c) Coulomb friction model

Fig. 1: Hybrid analytical model for flexible robotic finger system with oblique impact

2.1 Control equations of a single beam element

The one-dimensional two-node Euler beam element is used to discrete the finger system with neglecting the inertial moment and shearing effect of the cross-section. The finger system is divided into N elements, and the deformation of a single Euler beam element is shown in Fig. 2.
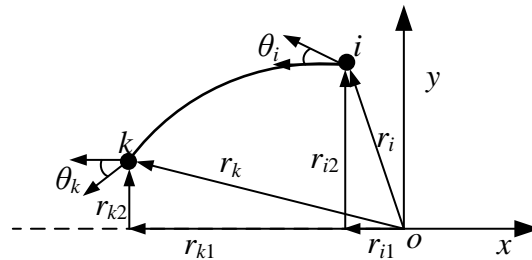

Fig. 2 The deformation of a single Euler beam element

2

The global position vector r for an arbitrary point on the Euler beam element is expressed as

$$r = Sq_e \tag{1}$$

where q_e is the vector of element nodal co-ordinates:

$$
\begin{aligned}
q_e &= \begin{bmatrix} q_1 & q_2 & q_3 & q_4 & q_5 & q_6 & q_7 & q_8 \end{bmatrix}^{\mathrm{T}} \\
&= \begin{bmatrix} r_{i1} & r_{i2} & \dfrac{\partial r_{i1}}{\partial x} & \dfrac{\partial r_{i2}}{\partial x} & r_{k1} & r_{k2} & \dfrac{\partial r_{k1}}{\partial x} & \dfrac{\partial r_{k2}}{\partial x} \end{bmatrix}^{\mathrm{T}}
\end{aligned} \tag{2}
$$

S is the global shape function which has a complete set of rigid-body modes, and it can be written as

$$S = \begin{bmatrix} s_1 l & 0 & s_2 l & 0 & s_3 l & 0 & s_4 l & 0 \\ 0 & s_1 l & 0 & s_1 l & 0 & s_3 l & 0 & s_4 l \end{bmatrix} \tag{3}$$

where the functions $s_i = s_i(\xi)$ ($i=1,2,3,4$) are defined as

$$s_1 = 1 - 3\xi^2 + 2\xi^3, \quad s_2 = l(\xi - 2\xi^2 + \xi^3), \quad s_3 = 3\xi^2 - 2\xi^3, \quad s_4 = l(\xi^3 - \xi^2) \tag{4}$$

and $\xi = x/l$. The kinetic energy T_e of the element can be written as

$$T_e = \frac{1}{2} \int_V \rho \dot{r}^{\mathrm{T}} \dot{r} \, dV = \frac{1}{2} \dot{q}_e^{\mathrm{T}} M_e \dot{q}_e \tag{5}$$

where M_e is mass matrix, which can be written as

$$M_e = \int_0^l \rho A S^{\mathrm{T}} S \, dx \tag{6}$$

here, ρ and A, respectively, are the density and cross section of the flexible link.

The strain energy U_e of the element is

$$U_e = U_1 + U_t = \frac{1}{2} \int_0^l \left[EA\varepsilon_1^2 + EI\kappa^2 \right] dx = \frac{1}{2} q_e^{\mathrm{T}} \left(K_1 + K_t \right) q_e \tag{7}$$

where E is Young's modulus, I is the inertial moment of cross-sectional area. U_1 and U_t are the longitudinal strain energy and transversal strain energy of the Euler beam element, respectively. And the longitudinal strain ε_1 and curvature κ are described in following equation

$$\begin{cases} \varepsilon_1 = \dfrac{1}{2}\left(q_e^{\mathrm{T}} S_1 q_e - 1 \right) \\ \kappa^2 = q_e^{\mathrm{T}} S''^{\mathrm{T}} S'' q_e \end{cases} \tag{8}$$

where $S_1 = S'S$. Therefore the longitudinal stiffness matrix K_1 and transversal stiffness matrix K_t are described as

$$K_1 = \frac{1}{2} EA\left(\int_0^l S_1 q_e q_e^{\mathrm{T}} S_1 dx - \int_0^l S_1 dx \right) \tag{9}$$

$$K_t = \int_0^l EI S''^{\mathrm{T}} S'' dx \tag{10}$$

Then the global stiffness matrix K_e is

$$K_e = K_1 + K_t \tag{11}$$

When the finger system and the rigid ground are in a separation stage, the flexible finger system is only affected by gravity, and the general external force matrix Q_e of the Euler beam element is

$$Q_e = \int_0^l \rho A S^{\mathrm{T}} \begin{bmatrix} 0 \\ g \end{bmatrix} dx \tag{12}$$

where g is the acceleration of gravity.

Subsequently, equations (5), (7) and (12) into the second Lagrange equation, the dynamic equation of the finite element can be obtained in a matrix form as

$$M_e \ddot{q}_e + K_e q_e = Q_e \tag{13}$$

where $\ddot{q}_e$ is the acceleration vector of the Euler beam element.

3

2.2 Control equations of flexible finger system

(1) Control equations

Based on the original dynamic equations, the differential algebraic equations of ANCF for multi-body system dynamics is derived by combining with the Lagrange multiplier method. The final dynamic equation is

$$\boldsymbol{M}\ddot{\boldsymbol{q}} + \boldsymbol{\Phi}^{\mathrm{T}}\boldsymbol{\lambda} + \boldsymbol{K}\boldsymbol{q} = \boldsymbol{Q} \tag{14}$$

where $\boldsymbol{M}$, $\boldsymbol{K}$ and $\boldsymbol{\Phi}$ are mass matrix, stiffness matrix and displacement's constraint matrix of the flexible finger system, respectively. $\boldsymbol{\lambda}$ is the Lagrange multiplier, $\boldsymbol{Q}$ is generalized external force. $\boldsymbol{q}$ is the generalized coordinates of the system.

When the fingertip and the rigid ground are in contact stage, the final dynamic equation will change, and it can be written as

$$\boldsymbol{M}\ddot{\boldsymbol{q}} + \boldsymbol{\Phi}^{\mathrm{T}}\boldsymbol{\lambda} + \boldsymbol{K}\boldsymbol{q} = \boldsymbol{Q}' \tag{15}$$

where

$$\boldsymbol{Q}' = \boldsymbol{Q} + \boldsymbol{F}_{\mathrm{c}} \tag{16}$$

where $\boldsymbol{F}_{\mathrm{c}}$ represents the contact forces, and it typically consists of normal and tangential contact forces. The normal and tangential contact forces can be calculated by the LCCM (see Fig. 1(b)) and Coulomb friction model (see Fig. 1(c)).

(2) Local complaint contact model (LCCM)

For the problem of fingertip contacts with the rigid ground, the contact points R and R' are located at the fingertip and the rigid ground, respectively (see Fig. 1(a)). The absolute displacement of contact point R is $\boldsymbol{U}_{\mathrm{R}} = \begin{bmatrix} x & y \end{bmatrix}^{\mathrm{T}}$ and the absolute displacement of contact point R is $\boldsymbol{U}_{\mathrm{R'}} = \begin{bmatrix} 0 & 0 \end{bmatrix}^{\mathrm{T}}$, the relative displacement between R and R' is $\boldsymbol{U}_{\mathrm{RR'}} = \begin{bmatrix} x & y \end{bmatrix}^{\mathrm{T}}$. Meanwhile, there exist a set of contact forces $\boldsymbol{F} = \begin{bmatrix} F_{\mathrm{t}} & F_{\mathrm{n}} \end{bmatrix}^{\mathrm{T}}$ and $\boldsymbol{F}' = \begin{bmatrix} F_{\mathrm{t}}' & F_{\mathrm{n}}' \end{bmatrix}^{\mathrm{T}}$ at the contact points R and R', respectively. Let the contact points first touch at an instance of time, $t=0$. The normal relative velocity between R and R', $\dot{y}(t)$, remains negative during the period of compression which ends at time t_{c} where $\dot{y}(t_{\mathrm{c}}) = 0$.

In the LCCM (see Fig. 1(b)), the bilinear compliant element in normal direction and linear compliant element in tangential direction are used to describe the deformation of the contact zone. These elements are connected to a massless particle P which can either stick or slide on the rigid ground. The absolute displacement of particle P is $\boldsymbol{U}_{\mathrm{P}} = \begin{bmatrix} u_x'' & u_y'' \end{bmatrix}^{\mathrm{T}}$, the relative displacement between R' and P is $\boldsymbol{U}_{\mathrm{PR'}} = \boldsymbol{U}_{\mathrm{P}} - \boldsymbol{U}_{\mathrm{R'}} = \begin{bmatrix} u_x'' & u_y'' \end{bmatrix}^{\mathrm{T}}$, and the relative displacement between R and P is $\boldsymbol{U}_{\mathrm{RP}} = \boldsymbol{U}_{\mathrm{R}} - \boldsymbol{U}_{\mathrm{P}} = \begin{bmatrix} u_x & u_y \end{bmatrix}^{\mathrm{T}}$, where u_x and u_y are the deformation of the normal and tangential compliant element. Let $v_{\mathrm{t}} = \dot{u}_x$ and $v_{\mathrm{n}} = \dot{u}_y$ in order to conveniently express the rate of extension of the compliant elements, $V_{\mathrm{t}} = \dot{x}$ and $V_{\mathrm{n}} = \dot{y}$ in order to conveniently express the rate of relative velocity between contact points R and R'.

The bilinear normal compliant element has stiffness k during an initial period of compression and subsequently, a stiffness $k e_*^{-2}$ during restitution (e_* is the Stronge's energetic coefficient of restitution). When the particle P is in slip state, the relationship between normal and tangential contact forces is governed the Coulomb law.

$$\begin{cases} F_{\mathrm{n}} = -k u_y & \left(0 < t < t_{\mathrm{c}} - \text{compression}\right) \\ F_{\mathrm{n}} = -k e_*^{-2} u_y + k(e_*^{-2} - 1) u_{\mathrm{yc}} & \left(t_{\mathrm{c}} < t < t_{\mathrm{f}} - \text{restitution}\right) \end{cases} \tag{17}$$

$$F_{\mathrm{t}} = -s \mu F_{\mathrm{n}} \quad \left(0 < t < t_f\right) \tag{18}$$

where t_{c} is the time of transition from compression to restitution, t_{f} is the time of separation, and $u_{\mathrm{yc}} = -k^{-1} F_{\mathrm{n}}(t_{\mathrm{c}})$ is the maximum normal compression. $s = \mathrm{sgn}(\dot{u}_x'') = \mathrm{sgn}(V_{\mathrm{t}} - v_{\mathrm{t}})$ represents the motion direction of the particle P. And $\dot{u}_x''$ is the velocity of the particle P. μ is the coefficient of friction between the particle P and the rigid ground.

When the particle P is in stick state, the tangential contact force is

$$F_t = -k\eta^{-2}u_x \quad \left(0 < t < t_f\right) \tag{19}$$

where η^{-2} is the ratio of tangential to normal stiffness. Formula (17) gives the loading-unloading hysteresis loop of the normal contact force as shown in Fig. 3. And the hysteresis of normal force results in a terminal indentation $u_y\left(t_f\right) = \left(1 - e_*^{-2}\right)u_{yc}$.

It should be noted that the large bending compliance of the finger structure leads to the deformation of the local contact zone in the normal direction frequently occur multiple transitions between compression and restitution before separation. The slope of the curve of force-deflection for the subseqent compression and restitution is the same as those for the first compression and restitution, respectively.
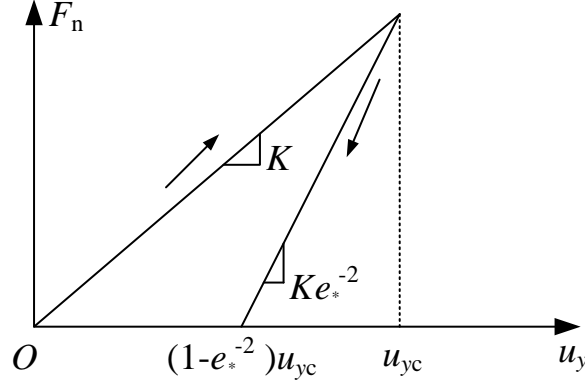

Fig. 3: Force-deflection relations for normal compliant element

3   Criteria for different motion processes and numerical integration method

3.1   Criteria for different motion processes

When the finger system falls freely from the initial position to a collision with a rigid ground, there will be a transition between slip and stick state in tangential direction as well as a transition between the compression and restitution state in normal direction. When the fingertip's tangential direction is in slip state and normal direction is in compression state, we call the fingertip is in the state of slip compression.

Here we assume the impact begins at time $t=0$. The following criteria can be used to determine the initial state of the system, the transition time t_c from compression to restitution, the transition time t_{01} from stick to slip and the transition time t_{10} from slip to stick, respectively.

(1)   Free falling

When the finger system is in free falling, the value of normal position for fingertip is must less than the falling height H,

$$|y| < H \tag{20}$$

(2)   Initial state

At initial time ($t=0$), the contact is in compression and either initial stick or slip. With the Amontons-Coulomb friction law, an upper bound on the angle of incidence for initial stick can be obtained by assuming initial slip and finding the time t_{10} when initial slip is brought to rest. Then taking the limit as t_{10} close to0, the upper limit of the ratio of tangential to normal incident velocity for initial stick is obtained. The upper bound for initial stick is

5

$$\left|V_t(0)/V_n(0)\right| < \mu\eta^2 \tag{21}$$

(3)   Compression or restitution

In the initial period of impact, the contact is in compression. Compression ends and restitution begins at a transition time t_c when the normal relative velocity vanishes,

$$v_n(t_c) = 0 \tag{22}$$

(4)   Stick or slip

During stick $|F_t(t)| \leq \mu F_n(t)$. If the system is in a state of stick, the time of transition from stick to slip t_{01} can be obtained by finding the time when the ratio of tangential to normal contact force equals the coefficient of friction. In addition, stick-slip transition requires that at time t_{01}, continuation of stick would result in a ratio of forces outside the cone of friction

$$\left|\frac{F_t(t_{01})}{F_n(t_{01})}\right| = \mu, \ F_t(t_{01})\dot{F}_t(t_{01}) > 0 \tag{23}$$

Alternatively, if the system is in a state of slip, the time of transition from slip to stick t_{10}, is obtained by considering the speed of slip $\dot{x}(t)$ and finding the time when the speed of slip is slowed by friction until it vanishes t_{10},

$$u_x''(t_{10}) = V_t(t_{10}) - v_t(t_{10}) = 0 \tag{24}$$

(5)   Separation

At time t_f-ε the normal contact force is positive, $F_n(t_f$-$\varepsilon)>0$, where ε is a infinite small positive value. The impact terminates at time t_f when the normal contact force vanishes,

$$F_n(t_f) = 0 \tag{25}$$

3.2   Numerical integration method

For the equation (15), the generalized-α method is used to slove this equation in this paper. The recurrence formula of generalized-α method is

$$q_{n+1} = q_n + \dot{q}_n \Delta t + (0.5 - \beta)\Delta t^2 a_n + \beta \Delta t^2 a_{n+1} \tag{26}$$

$$\dot{q}_{n+1} = q_n + \Delta t(1-\gamma)a_n + \Delta t \lambda a_{n+1} \tag{27}$$

where Δt is the time step, $\alpha_m = (2\xi-1)/(\xi+1)$, and $\alpha_f = \xi/(\xi+1)$. Vector a has the following relations

$$\begin{cases} (1-\alpha_m)a_{n+1} + \alpha_m a_n = (1-\alpha_f)\ddot{q}_{n+1} + \alpha_f q_n \\ a_0 = \ddot{q}_0 \end{cases} \tag{28}$$

where $\beta=(1+\alpha_f-\alpha_m)^2/4$, $\gamma=0.5+\alpha_f-\alpha_m$. $\xi\in[0\ 1]$, is the spectral radius of the algorithm. The smaller the ξ, the higher the energy dissipation. When ξ is equal to zero, the system will produce maximum energy dissipation, and the generalized-α method will be degenerated to Newmark integration method; when ξ is equal to one, the system will maintain energy without dissipating, and the generalized-α method will be degenerated to gradient algorithm.

4   Numerical results

To analyze the influence of H, μ and e_* on the oblique impact event, we choose the three groups of flexible robotic finger system: 1) $H=0.96$m, 1.00m and 1.04m when $\mu=0.4$ and $e_*=1$; 2) $e_*=0.6$, 0.8 and 1 when $\mu=0.4$ and $H=1.00$m; 3) $\mu=0.4$, 0.6, 0.8, 1.2, 1.4 and 1.6 when $H=1.00$m and $e_*=1$. Meanwhile, the elastic modulus E,

the cross-sectional area A, the moment of inertia I, and the density ρ of links are 70GPa, $5\times10^{-4}m^2$, $2\times10^{-8}m^4$, 2700kg/m³, respectively. The length of i-th link l_i (i=1,2,3) is 0.4m.

4.1 Contact forces

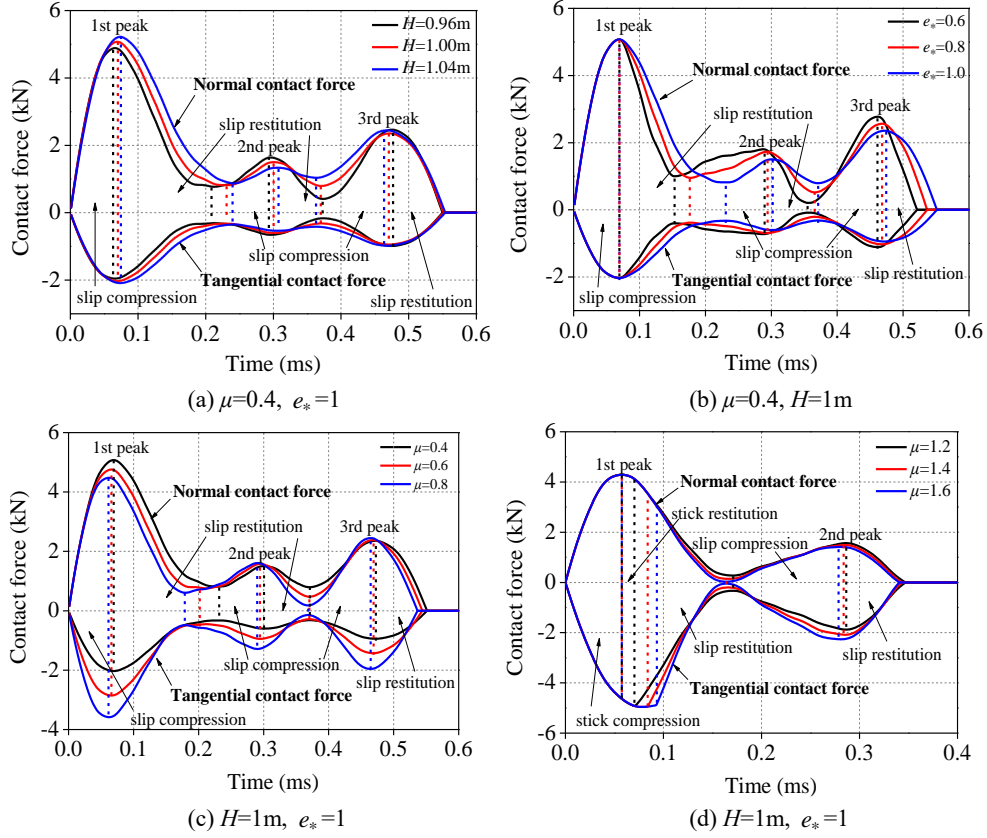Fig. 4: Normal and tangential contact forces

(a) μ=0.4, e_*=1
(b) μ=0.4, H=1m
(c) H=1m, e_*=1
(d) H=1m, e_*=1

Tab. 2: Peak value of contact forces

Contat forces (kN)	peak value	e_* (H=1m, μ=0.4)			H (μ=0.4, e_*=1)			μ (H=1m, e_*=1)					
		0.6	0.8	1.0	0.96m	1.00m	1.04m	0.4	0.6	0.8	1.2	1.4	1.6
F_n	1st	5.07	5.07	5.07	5.07	5.22	5.07	5.07	4.76	4.48	4.28	4.28	4.28
	2nd	1.80	1.73	1.50	1.50	1.33	1.50	1.50	1.58	1.61	1.56	1.49	1.42
	3rd	2.77	2.57	2.36	2.35	2.45	2.36	2.36	2.38	2.45	-	-	-
F_t	1st	2.03	2.03	2.03	2.03	2.09	2.03	2.03	2.85	3.58	4.92	4.96	4.96
	2nd	0.72	0.70	0.60	0.60	0.53	0.60	0.60	0.95	1.29	1.88	2.08	2.26
	3rd	1.11	1.03	0.94	0.94	0.98	0.94	0.94	1.43	1.96	-	-	-

Figs. 4(a), (b) are the normal and tangential contact force curves with parameters of groups 1) and 2), respectively. It is shown that each normal and tangential contact force curve has three peaks. Figs. 4(c) and (d) are the normal and tangential contact force curves with parameters of group 3). The results show that each normal and tangential contact force curve has three peaks when $\mu<0.8$, but the curve has two peaks when $\mu>1.2$. Tab. 2 is the peak value of contact forces. Fig. 4(a) shows that the 1st peak value of F_n and F_t will increase as increasing H. Comparing with those of H=0.96m, the 1st peak value will increase 4% for H=1m and 7% for H=1.04m. Moreover, the 2nd peak value of the F_n and F_t will increase as increasing H. The 3rd peak value will increase firstly, and then decrease as increasing H.

Fig. 4(b) shows that e_* has no strong influence on the 1st peak value of F_n and F_t, but the 2nd and 3rd peak value will be changed obviously. The reason is in the compression period of impact, e_* will not play any role when calculating F_n according to the formula (23).

Fig. 4(c) shows that the 1st peak value of F_n will decrease as increasing μ, on the contrary, the 1st peak value of F_t will increase as increasing μ. That is because the there is a large increment of μ, which leads to $F_c=\mu F_n$ still increases even though F_n decreases. Comparing with those of μ=0.4, when μ=0.6, the 1st peak value of F_n will decrease 6%, but the 1st peak value of F_t will increase 4%. When μ=0.8, the 1st peak value of F_n will decrease 12%, but the 1st peak value of F_t will increase 8%. The 2nd and 3rd peak value of F_n and F_t will increase with the increasing of μ. Be different from Fig. 4(c), Fig. 4(d) shows that the 1st peak value of F_n keeps invariant as increasing μ when $\mu \geq 1.2$. That is due to the fingertip is in the stick state during the initial period.

4.2 Multiple transitions between compression and restitution

(a) μ=0.4, e_*=1

(b) H=1m, μ=0.4
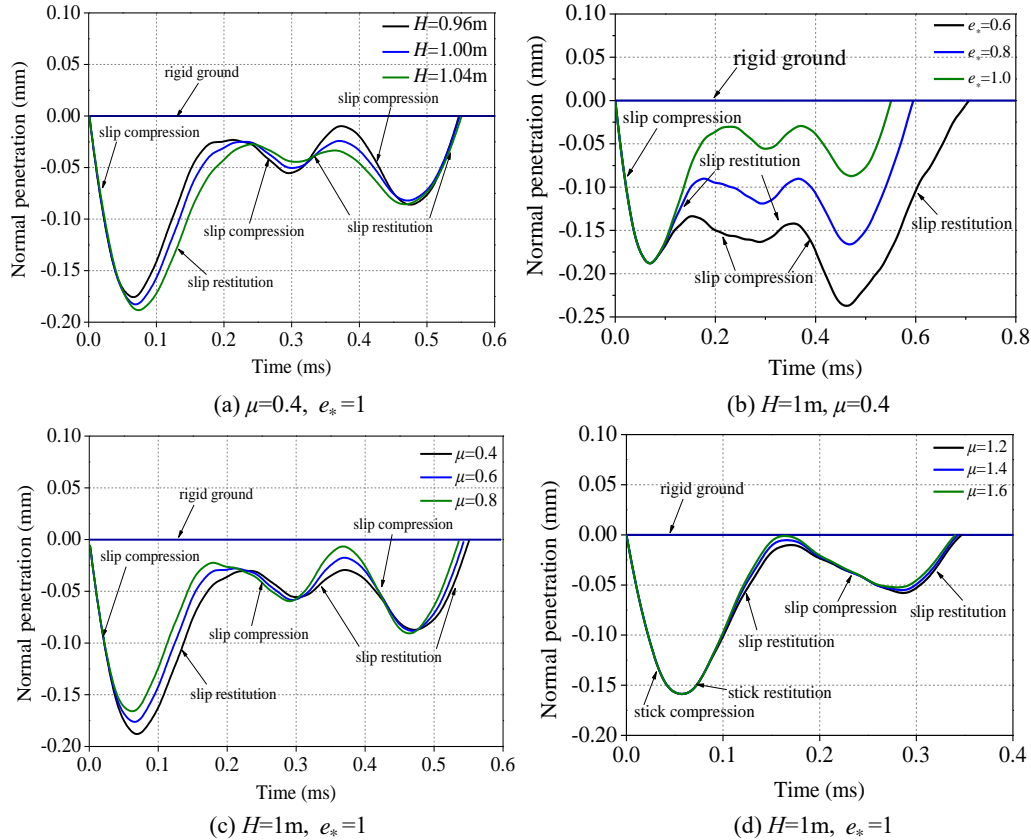
(c) H=1m, e_*=1

(d) H=1m, e_*=1

Fig. 5: Deformation curves of normal compliant element

Fig. 5 is the deformation curves of normal compliant element under different parameters. It is shown that when the deformation decreases, the fingertip is in the compression state, conversely, the fingertip is in restitution state. Figs. 5(a), (b) and (c) all show that the fingertip will experience three times transitions between compression and restitution in an oblique impact event, this is resulted from the structural bending compliance of the whole link. Fig. 5(d) shows that if it is in the stick state initially, the fingertip will only has two times transitions from compression and restitution.

From Fig. 5(b), it can be found that the 1st compression will experience the same time with different e_*, the duration time is 0.069ms. The duration times of the 1st restitution are 0.084ms for e_*=0.6, 0.108ms for e_*=0.8 and 0.162ms for e_*=1.0, respectively. Simultaneously, the duration times of the 2nd compression are 0.135ms for e_*=0.6, 0.177ms for e_*=0.8 and 0.068ms for e_*=1.0, respectively. The duration times of the 2nd restitution are 0.068ms for e_*=0.6, 0.072ms for e_*=0.8 and 0.071ms for e_*=1.0, respectively. The duration times of the 3rd

compression are 0.206ms for e_*=0.6, 0.102ms for e_*=0.8, and 0.101ms for e_*=1.0, respectively. The duration times of the 3rd restitution are 0.244ms for e_*=0.6, 0.127ms for e_*=0.8 and 0.079ms for e_*=1.0, respectively.
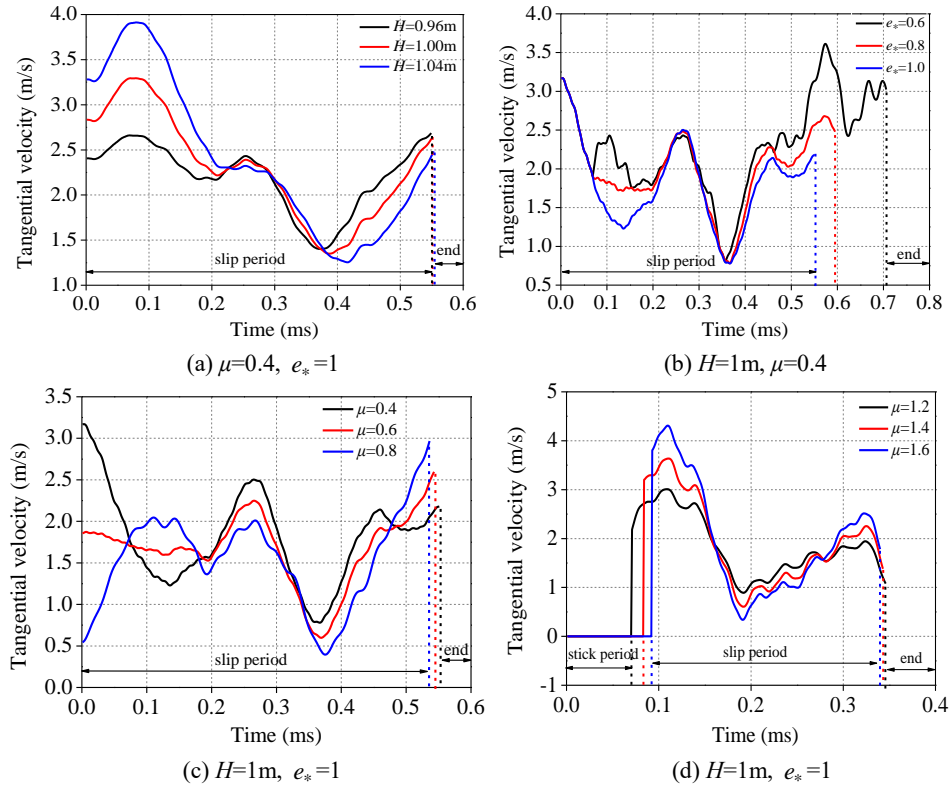
4.3 Stick-slip motion and trajectory of fingertip

(a) μ=0.4, e_*=1   (b) H=1m, μ=0.4

(c) H=1m, e_*=1   (d) H=1m, e_*=1

Fig. 6: Tangential velocity of particle P

Fig. 6 is the tangential velocity curves of particle P. According to Section 3.1, when the tangential velocity of particle P is equal to zero, the fingertip is in the stick state, conversely, it is in slip state. Figs. 6(a), (b) and (c) all show that the fingertip is always in slip state. Fig. 6(d) shows that the fingertip is in the stick state in the intial period. Meanwhile, Fig. 6(d) shows that the duration time of stick state will increase as increasing μ. Concretely, the duration time is 0.07ms for μ=1.2, 0.083ms for μ=1.4 and 0.092ms for μ=1.6, respectively.
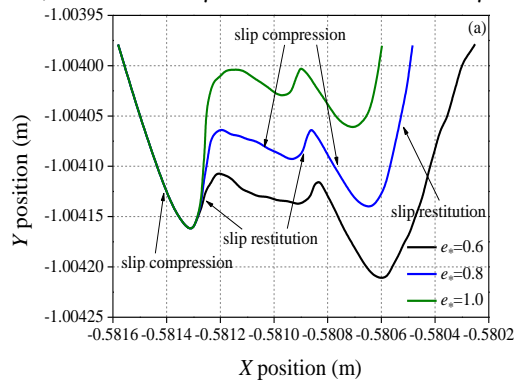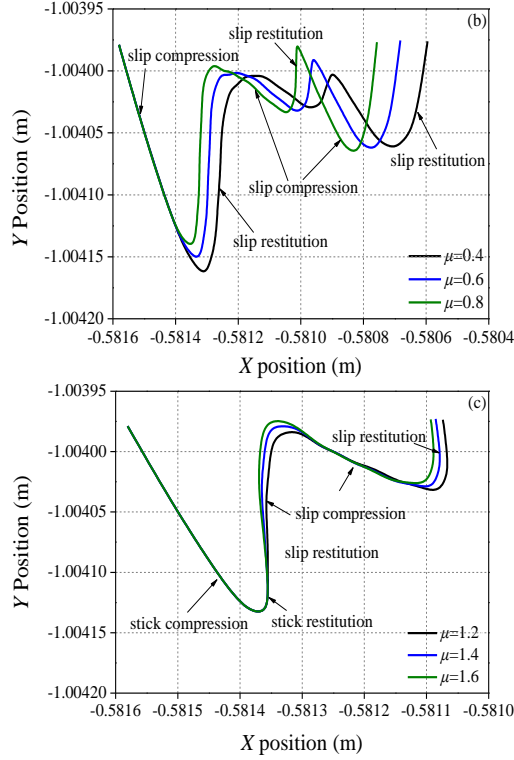
Fig. 7: Trajectory of fingertip((a) H=1, μ=0.4 (b) H=1m, e_*=1 (c) H=1m, e_*=1)

Fig. 7 is the trajectory of fingertip under different parameters. When the absolute position of Y direction decreaes, the fingertip is in a compression state, and when the absolute position of Y direction starts increasing, fingertip will enter into the restitution state. The sliding distance of fingertip before separation will decrease as increasing e_* and μ.

5   Conclusions

Considering the normal contact compliance and tangential contact compliance, a hybrid analytical model is proposed to study the oblique impact of the flexible robotic finger system in this paper. The absolute nodal coordinate formulation (ANCF) is used to discrete the deformation field and inertia filed of the finger structure. The numerical result shows that be different from the hard body, the large structural compliance of the finger cause the normal relative motion will experience multiple transitions between the compression state and the restitution state during an oblique impact event. There are two motion modes: 1) three times of slip compression-slip restitution when μ<0.8; 2) stick compression-stick restitution-slip restitution-slip compression-slip restitution when μ≥1.2.

Moreover, the results also show that the 1st peak value of the normal contact force will decrease as increasing μ when μ<0.8, on the contrary, the 1st peak value of the tangential contact force will increase. It also can be found that the 1st peak value of the normal and tangential contact forces will increase as increasing H. e_* has no effect on the 1st peak value of contact force, but the 2nd and 3rd peak value will be changed obviously. Besides, the duration time of an oblique impact event will decrease as increasing μ or decreasing H and e_*. The last, the sliding distance of fingertip before separation will decrease as increasing e_* and μ.

Acknowledgements

References

[1] P. Kuo and A. Deshpande, "A Novel Joint Design for Robotic Hands with Human-like Nonlinear Compliance," *Journal of Mechanisms & Robotics*, vol. 8, no. 2, pp. 1-10, 2015.

[2] J. Xie, W. Ding, "Hopf-Hopf bifurcation and invariant torus T^2 of a vibro-impact system," *International Journal of Non Linear Mechanics*, vol. 40, no. 4, pp. 531-543, 2005.

[3] E. Dimitrakopoulos, "Analysis of a frictional oblique impact observed in skew bridges," *Nonlinear Dynamics*, vol. 60, no. 4, pp. 575-595, 2010.

[4] Y. Zhang, Y. Long and et al, "Application of oblique impact theory of detonation waves at the explosive-metal interface in design of shaped charge," *Journal of Vibration & Shock*, vol. 30, no. 7, pp. 214-204, 2011.

[5] S Djerassi, "Stronge's hypothesis-based solution to the planar collision-with-friction problem," *Multibody System Dynamics*, vol. 24, no. 4, pp. 493-515, 2010.

[6] F. Pfeiffer, "Energy considerations for frictional impacts," *Archive of Applied Mechanics*, vol. 80, no. 1, pp. 47-56, 2010.

[7] Y. Shen and W. Stronge, "Painlevé paradox during oblique impact with friction," *European Journal of Mechanics/A*, vol. 30, no.4, pp. 457-467, 2011.

[8] L. Zaidi, J. Corrales and et al, "Model-based strategy for grasping $3D$ deformable objects using a multi-fingered robotic hand," *Robotics & Autonomous Systems*, vol. 95, pp. 196-206, 2017.

[9] Y. Shen and J.Gu, "Research on rigid body-spring-particle hybrid model for flexible beam under oblique impact with friction," *Journal of Vibration Engineering*, vol. 29, no. 1, pp. 1-7, 2016.